SUPPLEMENTARY INFORMATION

Conversion and conservation of light energy in a photosynthetic microbial mat ecosystem

Mohammad Al-Najjar[1], Dirk de Beer[1], Bo Barker Jørgensen[1], Michael Kühl[2], Lubos Polerecky[1]

[1]*Max-Planck Institute for Marine Microbiology, Celsiusstrasse 1, D-28359 Bremen, Germany;*
[2]*Marine Biological Laboratory, Department of Biology, University of Copenhagen, Strandpromenaden 5, DK–3000 Helsingør, Denmark*

Content

1 Sampling

Microbial mats originated from the coast of Sadeyat Island, near Abu Dhabi, United Arab Emirates (24° 31' 20" N, 54° 26' 50" E). Under natural conditions, the mat is exposed to continuous flushing by tidal seawater for ∼4 h a day, followed by calm periods during which water evaporates, resulting in daily salinity changes in the overlaying water between 35 and > 170. Several cm^2 of mats were collected in September 2007 at the onset of low tide (*in-situ* salinity of 90–130, temperature 35°C). The collected mat pieces were brought to the laboratory and incubated in filtered seawater (temperature 28°C, salinity of 33) under a 10h light / 14h dark illumination regime (incident quantum irradiance 480 μmol photon m^{-2} s^{-1}; light source AQUALINE 10000, MH 400W, spectrum similar to sunlight). During incubation, the evaporated water was replaced every 2–3 days to mimic environmental conditions.

2 Experimental setup and procedures

A microbial mat sample was placed in a small flow-chamber (11 cm × 4.5 cm × 5 cm) connected with plastic tubing to a peristaltic pump (Minipuls 3, Gilson), which maintained a stable laminar flow of filtered aerated seawater from a thermostated reservoir (temperature 23°C, salinity 35) above the mat surface. The flow cell was fixed on a holder and placed under a vertically incident collimated light beam from a tungsten-halogen lamp (KL 2500, Schott) equipped with an infrared (IR) cut off filter.

This ensured that the energy budget assessment involved only oxygenic photosynthesis, and prevented the activation of anoxygenic phototrophs, whose IR light-induced change in respiration could lead to overestimation of gross photosynthesis (Polerecky et al. 2007). It also avoided non-specific warming of the sample and the overlying water, which would otherwise hamper correct interpretation of the temperature measurements.

Oxygen concentration was measured with a fast-responding Clark-type O_2 microelectrode (tip diameter $\sim$30 μm) equipped with a guard cathode (Revsbech 1989). The sensor was linearly calibrated using signals measured in the anoxic layer of the mat and in the aerated overlaying seawater, and by applying temperature- and salinity-corrected O_2 solubility (Sherwood et al. 1991). Volumetric rates of gross photosynthesis (P in μmol O_2 m^{-3} s^{-1}) were measured by the light-dark shift method (Revsbech and Jørgensen 1983) using $\sim$3 s intermittent darkening periods to quantify the immediate O_2 depletion rate, which equals to the local rate of PS just before darkening. Measurements were conducted in vertical depth intervals of 100 μm, with 3 replicates at each depth. No immediate response in the O_2 signal upon darkening indicated a zero photosynthesis rate, i.e., the upper or lower boundary of the euphotic zone. Areal rates of gross photosynthesis (P_a in μmol O_2 m^{-2} s^{-1}) were calculated by integrating the volumetric rates over the depth of the euphotic zone (Polerecky et al. 2007).

A thermocouple microsensor (TP50) with a tip diameter of 50 μm was connected to a thermocouple meter (T30, both from Unisense A/S) and used to measure steady state temperature microprofiles inside and above the illuminated mat. A two-point linear calibration after each measurement was done against a digital thermometer (GMH 3710, Greisinger Electronics) using warm and cold tap water.

Gross PS and temperature measurements were conducted at increasing incident quantum irradiances of 20–1300 μmol photon m^{-2} s^{-1}. The illumination at each irradiance level was kept constant for up to 1 h to reach steady state O_2 conditions, which was determined from the microsensor signal before each measurement. To prevent self-shading and allow simultaneous measurements, the O_2 and thermocouple microsensors were positioned at zenith angles of 135° and −135°, respectively, relative to the vertically incident light. The measuring tips of both microsensors were positioned at the mat surface and in close proximity to each other using a 3-axis manual micromanipulator aided by observation under a dissection microscope (SV6, Zeiss).

Light attenuation in the mat was measured using a fiber-optic scalar irradiance microprobe (Lassen et al. 1992b) connected to a spectrometer (USB4000, Ocean Optics). The sensor had a $\sim$100 μm wide white integrating sphere casted onto the tapered fiber tip. Scalar irradiance microprofiles were measured in three different spots, normalized at each wavelength to the scalar irradiance at the mat surface, and averaged. This was done for several incident quantum irradiances in the range of 20–1000 μmol photon m^{-2} s^{-1}.

The spectral quantum irradiance of the incident light was measured with a spectrometer (USB4000, Ocean Optics) equipped with an optical fiber (QP200-2-VIS/BX, Ocean Optics) and a cosine collector (CC3, Ocean Optics). The collector was fixed through a hole at the bottom of a small cell at an identical distance as the mat surface, and faced the light source. The spectral signal measured by the cosine collector represented the relative spectral quantum irradiance (F_λ, in counts m^{-2} s^{-1} nm^{-1}) in the wavelength interval from λ to $\lambda + d\lambda$, where λ ranged from 350 to 1000 nm. To quantify the real spectral quantum irradiance (I_λ, in μmol photon m^{-2} s^{-1} nm^{-1}), the signal was intercalibrated against a PAR quantum irradiance sensor (QUANTUM, LI-COR Biosciences) connected to a light meter (LI-250, LI-COR Biosciences). First, F_λ was integrated over the wavelength interval of PAR (400–700 nm) and set equal to the quantum sensor reading. The resulting conversion factor was then used to multiply F_λ to obtain I_λ for all wavelengths in the PAR region.

A fiber-optic field radiance microsensor (Jørgensen and Marais 1988, Kühl and Jørgensen 1994) was used to quantify the spectral reflectance of the mat sample, R_λ. First, the mat sample was vertically illuminated with a broad-band incident light source (Schott KL2500, without the IR cut-off filter) and the reflected light, $I_{\lambda,\mathrm{mat}}$, was collected with the sensor oriented at $\sim$10° from the vertical. Then the mat sample was exchanged with a white reflectance standard (Spectralon, Labsphere) and the reference light intensity, $I_{\lambda,\mathrm{ref}}$, was recorded. Spectral reflectance was then calculated as $R_\lambda = I_{\lambda,\mathrm{mat}}/I_{\lambda,\mathrm{ref}}$, based on the assumption that the mat acts as a Lambertian diffuse reflector. Similar measurements were conducted to estimate the proportion of the incident light radiated back as auto-fluorescence by the light harvesting pigments. In this case, the mat sample was illuminated by a narrow-band light emitting diode (LED, Luxeon) through a short-pass excitation filter (Schott) and the emitted fluorescence was detected through a long-pass emission filter. Three combinations of the excitation LED's and cut-off filters were used: blue (Luxeon, LXHL-LR5C, $\lambda_{\max} = 450\,\mathrm{nm}$, $\lambda_{\mathrm{cut-off}} = 470\,\mathrm{nm}$), green (Luxeon, LXHL-LM3C, $\lambda_{\max} = 530\,\mathrm{nm}$, $\lambda_{\mathrm{cut-off}} = 600\,\mathrm{nm}$) and amber (Luxeon, LXHL-LL3C, $\lambda_{\max} = 590\,\mathrm{nm}$, $\lambda_{\mathrm{cut-off}} = 600\,\mathrm{nm}$). The amount of auto-fluorescence was then calculated as the ratio between the emitted and excitation light levels, where the latter was determined using the same setup but without the emission cut-off filter and with the mat sample exchanged by the white reflectance standard.

Data aquisition and measurement automation were done by a computer using custom-made programs m-Profiler, Spectral-m-Profiler, DAQ-server, LINPOS-server and G-Client. The analysis of the microsensor data was aided by the program mpr-plotter. Detailed description of the programs as well as of the hardware for microsensor measurements can be found at http://www.microsen-wiki.net/.

3 Model of the attenuation and absorption of light in a microbial mat

Photosynthetic quantum efficiency (QE) is defined as the rate of photosynthesis, P, per quantity of light absorbed, E_{abs}. Thus, the measurement of QE for a given system (e.g., a microbial mat) or its constituent (e.g., a phototrophic cell) requires the knowledge of P and E_{abs}. These parameters can be quantified either per volume, area or biomass of the studied system.

Microphytobenthic (MPB) systems such as photosynthetic microbial mats are highly packed and compact assemblages of photosynthetically active and inactive microbial cells and other biotic and abiotic components such as sediment particles, extracellular polymeric substances or detritus. Although all components contribute to light absorption in the system, only the photosynthetically active cells perform photosynthesis. Because of the high compaction, the measurements of photosynthesis and light absorption in MPB systems requires the use of specialized tools and approaches. For the measurement of photosynthesis, the microsensor-based light-dark shift method (Revsbech and Jørgensen 1983) has been widely used, as it allows quantification of volumetric gross photosynthesis rates (P in $\mu\mathrm{mol\,O_2\,m^{-3}\,s^{-1}}$) with a spatial resolution of 100–200 μm. For the assessment of light with a similar spatial resolution, fiber-optic based irradiance or scalar irradiance microprobes have been applied (Lassen et al. 1992b, Lassen and Jørgensen 1994, Kühl and Jørgensen 1994, Kühl et al. 1994). Although these measurements allow characterization of locally *available* photon fluxes, from which parameters such as the light attenuation coefficient can be derived, it is unclear how they can directly yield information on the locally *absorbed* light energy. This complication stems from the fact that scattering plays an important role in the way light propagates, attenuates and eventually becomes absorbed in microbial mats or other systems with high density of cells and other material. Kühl and Jørgensen (1994) proposed and realized a method for such a purpose. Their approach was, however, not straightforward, as it involved rather laborious and practically difficult measurements of angular distributions of light irradiances at various

depths in the mat, from which the locally absorbed light was then calculated. Here we propose a theoretical framework from which light propagation in photosynthetic microbial mats can be more easily understood, and which allows a more straightforward way to quantify absorbed light from parameters that are relatively simple to measure. The derivation adopts ideas of Yang et al. (2004) that were developed in their revision and application of the original Kubelka-Munk (K–M) theory of light propagation in a scattering and absorbing medium for ink-jet printing.

We assume that the light field in the mat is diffused, i.e., photons at each depth propagate with equal probability in all directions. As shown by Kühl and Jørgensen (1994), this is generally a good assumption for measurements where the mat is illuminated vertically by a collimated light beam from a lamp, except for the very top mat layer (100–200 μm), where the incident light undergoes a transition from a collimated to diffused light field (see below).

The light field in the mat is divided into two components, a downwelling photon flux, F_+, associated with photons traveling in the positive z-direction, and an upwelling photon flux, F_-, associated with photons propagating in the negative z-direction (Fig. S1). By definition, these fluxes represent the amount of photons that pass through a horizontal plane of unit area per second, i.e., a quantity measured by a cosinus-corrected irradiance sensor. As suggested in the original K–M theory, scattering in the medium results in a transfer of energy from F_+ to F_- and vice versa, whereas absorption in the medium results in a loss of energy. The medium is assumed to be linear, i.e., the strengths of the energy transfer and loss are proportional to the photon flux. Thus, the spatial distribution of the two fluxes can be discribed by a set of coupled first-order linear differential equations,

$$\begin{aligned} \frac{\mathrm{d}F_+}{\mathrm{d}z} &= -(K+S)F_+ + SF_-, \\ -\frac{\mathrm{d}F_-}{\mathrm{d}z} &= -(K+S)F_- + SF_+, \end{aligned} \tag{1}$$

where K and S denote the absorption and scattering coefficient, respectively. As stressed by Yang et al. (2004), these parameters do *not* represent the intrinsic absorption and scattering properties of the material in which the light propagates, but are used only as phenomenological parameters describing the energy transfer efficiencies between the two light field components. However, a relationship between the phenomenological and intrinsic parameters can be found if the local angular distribution of light in the material is known (Yang et al. 2004). As we will show below, under certain conditions that are typically fulfilled in mats the knowledge of these intrinsic parameters is not required to find out the volumetric rates of light absorption.

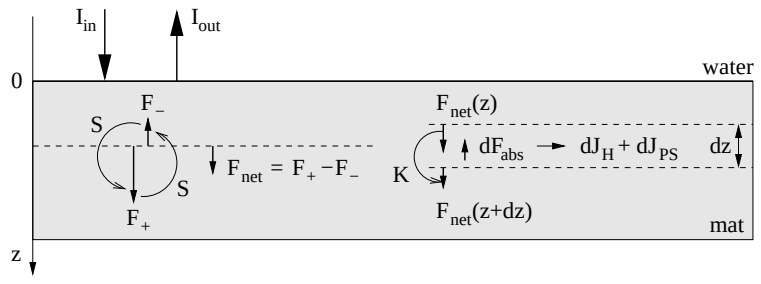

Fig. S 1: Schematic diagram of light propagation and utilization in a microbial mat. Photons are transferred between downwelling (F_+) and upwelling (F_-) fluxes due to scattering (S). The decrease in the net photon flux ($\mathrm{d}F_{\mathrm{net}}$) due to absorption ($K$) in the depth interval $\mathrm{d}z$ is partially conserved by photosynthesis ($\mathrm{d}J_{\mathrm{PS}}$) and partially dissipated as heat ($\mathrm{d}J_{\mathrm{H}}$).

It can easily be shown that a general solution to Eq. 1 takes the form

$$F_+(z) = b_+ e^{\alpha z} + b_- e^{-\alpha z},$$
$$F_-(z) = c_+ e^{\alpha z} + c_- e^{-\alpha z}, \tag{2}$$

where $b_\pm$ and $c_\pm$ are coefficients that depend on boundary conditions and

$$\alpha = \sqrt{K(K+2S)} \tag{3}$$

is the light attenuation coefficient (in mm^{-1}). Equation 2 states that the downwelling and upwelling fluxes consist of two components, one exponentially increasing and the other one exponentially decreasing with depth in the medium.

In the following we assume that a diffused incident light beam characterized by irradiance I_{in} (in $\mathrm{J\,m^{-2}\,s^{-1}}$) enters the microbial mat from above at its surface $z = 0$ (i.e., there is no input of light from below or within the mat). We also assume that the mat is homogenous, spreads over a semifinite space $z \geq 0$, and is covered by water from above ($z < 0$) where no scattering or absorption takes place. Based on these assumptions it follows from Eq. 2 that (i) to avoid infinities, the amplitudes of the exponentially increasing fluxes must equal zero ($b_+ = c_+ = 0$), and (ii) the light field at the mat surface consists of a downwelling flux equal to I_{in} and an upwelling flux denoted as I_{out}. We define the upwelling flux by means of reflectance, R, as

$$I_{\mathrm{out}} = R I_{\mathrm{in}}. \tag{4}$$

Thus, the light field at any depth in the mat is written as

$$F_+(z) = I_{\mathrm{in}} e^{-\alpha z},$$
$$F_-(z) = R I_{\mathrm{in}} e^{-\alpha z}. \tag{5}$$

The central question of how much light is *absorbed* at a given depth in the mat is approached by considering the following mass balance. The net downwelling photon flux at depth z, i.e., the amount of photons passing through a horizontal area at depth z per unit time, is given by the difference between the downwelling and upwelling fluxes, $F_{\mathrm{net}}(z) = F_+(z) - F_-(z)$. Thus, the photon flux lost (absorbed) in an infinitesimally small depth interval $\langle z, z + \mathrm{d}z\rangle$ equals to the difference between the net photon fluxes at the boundaries of the interval,

$$\mathrm{d}F_{\mathrm{abs}} = F_{\mathrm{net}}(z + \mathrm{d}z) - F_{\mathrm{net}}(z). \tag{6}$$

One could consider that, due to auto-fluorescence of pigments, photons are also being generated inside the mat in addition to being scattered and absorbed. However, this phenomenon results in a transformation of shorter-wavelength photons to longer-wavelength photons, and is therefore already included in the present formalism. Following the definition of F_{net} (Eq. 6) and applying Eq. 1, the volumetric rate of photon absorption at depth z satisfies equation

$$\frac{\mathrm{d}F_{\mathrm{abs}}}{\mathrm{d}z} = \frac{\mathrm{d}F_{\mathrm{net}}}{\mathrm{d}z} = -K(F_+ + F_-). \tag{7}$$

Until now, the reflectance R was only a postulated parameter. Now we show that it can be derived by considering the total photon mass balance. Specifically, the total amount of photons lost in the mat is obtained by integrating the volumetric rate given by Eq. 7 over the entire depth of the mat, $z \in \langle 0, \infty)$. Upon substitution from Eq. 5, this gives

$$F_{\mathrm{abs,tot}} = \int_0^\infty \frac{\mathrm{d}F_{\mathrm{abs}}}{\mathrm{d}z}\mathrm{d}z = \frac{K}{\alpha}(1+R)I_{\mathrm{in}}. \tag{8}$$

Since at the mat surface the difference between the total downwelling photon flux, I_{in}, and the total upwelling photon flux, RI_{in}, must be equal to the total photon flux lost in the mat, we can immediately see that

$$I_{\mathrm{in}} - RI_{\mathrm{in}} = F_{\mathrm{abs,tot}} \qquad \Rightarrow \qquad R = \frac{\alpha - K}{\alpha + K}. \tag{9}$$

This shows that, assuming that the reflection due to refractive index mismatch between the mat and the overlying water is zero, the reflectance of the mat is zero if $\alpha = K$, or, using Eq. 3, if $S = 0$. In other words, if there were no light scattering in the mat, the upwelling flux would be zero and the mat would appear black.

Experimentally, scalar irradiance, E_s, can be measured in intact mat samples with a high spatial resolution using a scalar irradiance fiber-optic microprobe (Lassen et al. 1992a). However, Eq. 7 shows that it is the sum of downwelling and upwelling cosine-corrected photon fluxes, i.e., the down- and upwelling irradiances, that needs to be measured to quantify the locally absorbed light. While irradiance microsensors have been developed (Lassen and Jørgensen 1994, Kühl et al. 1994), such microscale irradiance measurements are practically difficult to obtain. The assumption that the light field in the mat is diffused allows quantification of $F_+ + F_-$ from E_s. This follows straightforwardly from the definition of the light fluxes. For a diffused light field, the ratio between E_s and $F_+ + F_-$ is

$$f = \frac{E_s}{F_+ + F_-} = \frac{\int_{4\pi} 1 \,\mathrm{d}\Omega}{\int_{4\pi} |\cos\theta| \,\mathrm{d}\Omega} = 2. \tag{10}$$

In this equation, Ω and θ denote the solid and zenith angle, respectively. Combining Eqs. 5 and 10, it is easy to see that the depth profile of scalar irradiance in diffuse light field follows an exponentially decreasing function

$$E_s(z) = 2(F_+(z) + F_-(z)) = 2I_{\mathrm{in}}(1 + R)e^{-\alpha z}. \tag{11}$$

This equation has very important practical implications. First, by measuring the attenuation of the *scalar* irradiance in the mat, the attenuation coefficient α can be quantified by taking the slope of the line $\ln E_s(z)$ vs. z (recall that the mat is assumed to be homogeneous in this derivation). Then, using a cosine-corrected sensor, one can easily determine the mat irradiance reflectance (see Eq. 4). Consequently, the parameter K can be calculated as

$$\boxed{K = \alpha \frac{1 - R}{1 + R},} \tag{12}$$

as follows from Eq. 9. Taking into account Eq. 7, these steps thus allow calculation of the locally *absorbed* light from the locally *available* light, i.e., the measured scalar irradiance $E_s(z)$, as

$$\boxed{\frac{\mathrm{d}F_{\mathrm{abs}}(z)}{\mathrm{d}z} = \frac{K}{2} E_s(z).} \tag{13}$$

It should be emphasized that $\mathrm{d}F_{\mathrm{abs}}(z)/\mathrm{d}z$ represents the local *density* of the absorbed light energy, i.e., it is a volumetric quantity (in $\mathrm{J\,m^{-3}\,s^{-1}}$), whereas $E_s(z)$ is the local *flux* of light energy, i.e., an aereal quantity (in $\mathrm{J\,m^{-2}\,s^{-1}}$).

Finally, by defining the local QE of a mat volume at depth z, $\eta(z)$, as a ratio between the local volumetric rate of photosynthesis, $P(z)$, and the volumetric rate of light absorption, $\mathrm{d}F_{\mathrm{abs}}(z)/\mathrm{d}z$, an explicit formula for $\eta(z)$ is obtained:

$$\boxed{\eta(z) = \frac{2P(z)}{K E_s(z)}.} \tag{14}$$

This formula contains only quantities that can be directly experimentally measured, and thus has a very practical application.

It is important to note, however, that Eq. 14 yields QE for a given *volume* that can be resolved by the oxygen and light microsensor measurements. Because this volume may contain components that absorb light but do not evolve O_2, Eq. 14 may underestimate the true QE of the photosynthetically active cells in that volume. Furthermore, microscale light measurements in microbial mats illuminated by colimated light typically show an increase in the scalar irradiance within the uppermost 100–200 μm of the mat (Lassen et al. 1992b, Lassen and Jørgensen 1994, Kühl and Jørgensen 1994, Kühl et al. 1994). This, seemingly, does not agree with the concept of an exponentially decreasing light field employed here (e.g., an increasing light field would imply negative α in Eq. 5, which would then lead to negative values for K and η). However, it is important to realize that, under such illumination, the light field corresponding to the photons traveling in the downward direction changes from a collimated one immediately under the mat surface to a diffusive one within the top 100–200 μm (Kühl and Jørgensen 1994). This change is, presumably, the reason why the signal measured by the scalar irradiance microsensor first increases in this depth interval before it starts exponentially decreasing below, as assumed in the formalism employed here. However, to prove this by a rigorous theoretical approach would go far beyond the scope of this study. Thus, strictly speaking, Eq. 14 for the local photosynthetic efficiency is not valid for the uppermost transitional mat layer where the light field is anisotropic. Nevertheless, from a practical point of view, Eq. 14 can be used as a good approximation for the local photosynthetic efficiency also for the transitional layer, combining the scalar irradiance measured *in* that layer with the parameter K determined from the light measurements *below*.

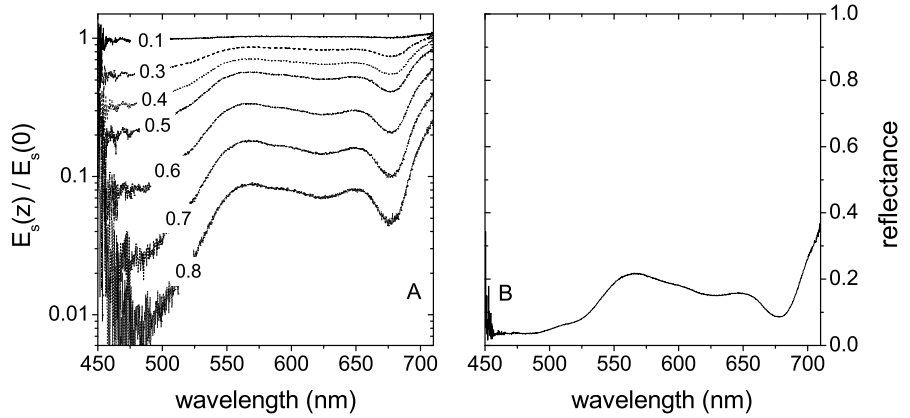

Fig. S 2: Optical properties of the studied microbial mat. (A) Scalar irradiance at various depths (numbers in mm) inside the mat as a function of wavelength, normalized to the scalar irradiance at the mat surface. (B) Spectral reflectance of the mat, i.e., the ratio between the back-scattered and incident irradiance.

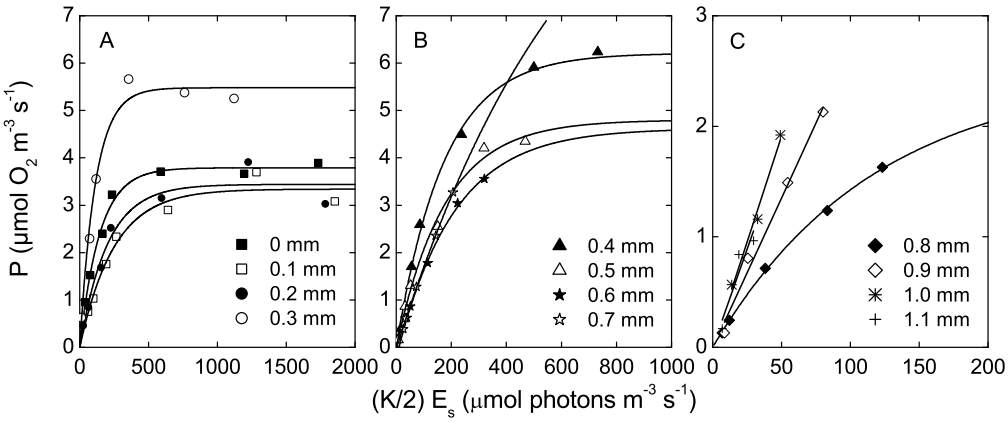

Fig. S3: Volumetric rates of gross photosynthesis at various depths inside the studied microbial mat as a function of the locally absorbed light density, calculated from the locally available scalar irradiance using Eq. 13. Lines depict the best fits by the saturated exponential function (Eq. 4 in the main text). Note different scaling of the axes.

Table. S1: Maximum quantum efficiency (QE_{max}) and energy efficiency (EE_{max}) of photosynthesis for different phototrophic organisms/systems

Measurement method	QE_{max} (O_2 photon^{-1})	EE_{max} (J/J) %	Organism/System	Source
O_2 evolution, chamber	0.012–0.111	2.65–24.4*	higher terrestrial plants (23 species)	Ref. 1
CO_2 assimilation, chamber	0.027–0.082	5.85–18.0*	higher terrestrial plants (40 species)	Ref. 1
biomass growth	0.021*	4.6	C3 plants	Ref. 2
biomass growth	0.027*	6.0	C3 plants	Ref. 2
pulse amplitude fluorimetry	0.049–0.110	10.7–24.2*	phytoplankton	Ref. 3
pulse amplitude fluorimetry	0.037–0.065	8.2–14.3*	freshwater and marine microalgae	Ref. 4
O_2 evolution, microsensors	0.05–0.07	10.7–15.4*	macroalgae	Ref. 5
O_2 evolution, microsensors	0.01–0.07	3.1–15.4*	freshwater submerged angiosperms	Ref. 5
recalculation of literature P-E curves	0.005–0.095	1.1–21*†	coral reef organisms (corals, various algae)	Ref. 6
O_2 evolution, microsensors	0.019	4.5	photosynthetic microbial mat	this work
O_2 evolution, microsensors	0.01–0.07	2.2–15.4*	microphytobenthic systems	Refs. 7–15
	0.00045*	0.1	primary production of the global ecosystem	Ref. 16
8 photons absorped per O_2 evolved	0.125	27.7*	theoretical maximum	Ref. 17

[1]Singsaas et al. (2001), [2]Zhu et al. (2008), [3]Dubinsky et al. (1986), [4]Flameling and Kromkamp (1998), [5]Frost-Christensen and Sand-Jensen (1992), [6]Hochberg and Atkinson (2008), [7]Lassen et al. (1992b), [8]Revsbech et al. (1983), [9]Kühl et al. (1996), [10]Epping and Jørgensen (1996), [11]Hawes and Schwarz (1999), [12]Epping and Kühl (2000), [13]Buffan-Dubau et al. (2001), [14]Jonkers et al. (2003), [15]Vopel and Hawes (2006), [16]Makarieva et al. (2008), [17]Falkowski and Raven (1997)

*Calculated based on Eq. 1 in the main text.

†Mean ± S.D. of $n = 106$ values: $QE_{max} = 0.0328 \pm 0.0189\,O_2$ photon^{-1}, $EE_{max} = 7.3 \pm 4.2$.

Supplementary References

Buffan-Dubau E., Pringault O., de Wit R. (2001). Artificial cold-adapted microbial mats cultured from Antarctic lake samples. 1. Formation and structure. *Aquatic Microbial Ecology* **26**(2):115–125.

Dubinsky Z., Falkowski P.G., Wyman K. (1986). Light harvesting and utilization by phytoplankton. *Plant and Cell Physiology* **27**(7):1335–1349.

Epping E., Kühl M. (2000). The responses of photosynthesis and oxygen consumption to short-term changes in temperature and irradiance in a cyanobacterial mat (Ebro Delta, Spain). *Environmental Microbiology* **2**(4):465–474.

Epping E.H.G., Jørgensen B.B. (1996). Light-enhanced oxygen respiration in benthic phototrophic communities. *Marine Ecology Progress Series* **139**(1-3):193–203.

Falkowski P.G., Raven J.A. (1997). *Aquatic Photosynthesis*. Blackwell Publishers.

Flameling I.A., Kromkamp J. (1998). Light dependence of quantum yields for PSII charge separation and oxygen evolution in eucaryotic algae. *Limnology and Oceanography* **43**(2):284–297.

Frost-Christensen H., Sand-Jensen K. (1992). The quantum efficiency of photosynthesis in macroalgae and sumberged angiosperms. *Oecologia* **91**(3):377–384.

Hawes I., Schwarz A.M. (1999). Photosynthesis in an extreme shade environment: Benthic microbial mats from Lake Hoare, a permanently ice-covered Antarctic lake. *Journal of Phycology* **35**(3):448–459.

Hochberg E.J., Atkinson M.J. (2008). Coral reef benthic productivity based on optical absorptance and light-use efficiency. *Coral Reefs* **27**(1):49–59.

Jonkers H.M., Ludwig R., De Wit R., Pringault O., Muyzer G., Niemann H., Finke N., De Beer D. (2003). Structural and functional analysis of a microbial mat ecosystem from a unique permanent hypersaline inland lake: 'La Salada de Chiprana' (NE Spain). *FEMS Microbiology Ecology* **44**(2): 175–189.

Jørgensen B.B., Marais D.J.D. (1988). Optical-properties of benthic photosynthetic communities—fiber-optic studies of cyanobacterial mats. *Limnology and Oceanography* **33**(1):99–113.

Kühl M., Jørgensen B.B. (1994). The light-field of microbenthic communities—radiance distribution and microscale optics of sandy coastal sediments. *Limnology and Oceanography* **39**(6):1368–1398.

Kühl M., Lassen C., Jørgensen B.B. (1994). Light penetration and light intensity in sandy marine sediments measured with irradiance and scalar irradiance fiber-optic microprobes. *Marine Ecology Progress Series* **105**(1-2):139–148.

Kühl M., Glud R.N., Ploug H., Ramsing N.B. (1996). Microenvironmental control of photosynthesis and photosynthesis-coupled respiration in an epilithic cyanobacterial biofilm. *Journal of Phycology* **32**(5): 799–812.

Lassen C., Jørgensen B.B. (1994). A fiberoptic irradiance microsensor (cosine collector)—application for in-situ measurements of absorption-coefficients in sediments and microbial mats. *FEMS Microbiology Ecology* **15**(3-4):321–336.

Lassen C., Ploug H., Jørgensen B.B. (1992)a. A fiberoptic scalar irradiance microsensor—application for spectral light measurements in sediments. *FEMS Microbiology Ecology* **86**(3):247–254.

Lassen C., Ploug H., Jørgensen B.B. (1992)b. Microalgal photosynthesis and spectral scalar irradiance in coastal marine-sediments of Limfjorden, Denmark. *Limnology and Oceanography* **37**(4):760–772.

Makarieva A.M., Gorshkov V.G., Li B.L. (2008). Energy budget of the biosphere and civilization: Rethinking environmental security of global renewable and non-renewable resources. *Ecological Complexity* **5**(4):281–288.

Polerecky L., Bachar A., Schoon R., Grinstein M., Jørgensen B.B., de Beer D., Jonkers H.M. (2007). Contribution of Chloroflexus respiration to oxygen cycling in a hypersaline microbial mat from Lake Chiprana, Spain. *Environmental Microbiology* **9**(8):2007–2024.

Revsbech N.P. (1989). An oxygen microsensor with a guard cathode. *Limnology and Oceanography* **34** (2):474–478.

Revsbech N.P., Jørgensen B.B. (1983). Photosynthesis of benthic microflora measured with high spatial-resolution by the oxygen microprofile method—capabilities and limitations of the method. *Limnology and Oceanography* **28**(4):749–756.

Revsbech N.P., Jørgensen B.B., Blackburn T.H., Cohen Y. (1983). Microelectrode studies of the photosynthesis and O2, H2S, and pH profiles of a microbial mat. *Limnology and Oceanography* **28**(6): 1062–1074.

Sherwood J.E., Stagnitti F., Kokkinn M.J., Williams W.D. (1991). Dissolved-oxygen concentrations in hypersaline waters. *Limnology and Oceanography* **36**(2):235–250.

Singsaas E.L., Ort D.R., DeLucia E.H. (2001). Variation in measured values of photosynthetic quantum yield in ecophysiological studies. *Oecologia* **128**(1):15–23.

Vopel K., Hawes I. (2006). Photosynthetic performance of benthic microbial mats in Lake Hoare, Antarctica. *Limnology and Oceanography* **51**(4):1801–1812.

Yang L., Kruse B., Miklavcic S.J. (2004). Revised Kubelka-Munk theory. II. Unified framework for homogeneous and inhomogeneous optical media. *Journal of the Optical Society of America A—Optics Image Science and Vision* **21**(10):1942–1952.

Zhu X.G., Long S.P., Ort D.R. (2008). What is the maximum efficiency with which photosynthesis can convert solar energy into biomass? *Current Opinion in Biotechnology* **19**(2):153–159.